Auto-regulation and blood flow in the cerebral circulation

Tim David[1,*,†], Michael Brown[2,‡] and A. Ferrandez[3,§]

[1]*Department of Mechanical Engineering, University of Canterbury, Private Bag 4800, Christchurch, New Zealand*
[2]*School of Mechanical Engineering, University of Leeds, Woodhouse Lane, LEEDS, U.K.*
[3]*Sony Computer Entertainment Europe, 19-20 Park Row, Park Row House, 4th Floor, Leeds, LS1 5JF, U.K.*

SUMMARY

The application of computational fluid dynamics (CFD) to model biological flows is quite a recent one. This study presents a CFD model of the Circle of Willis developed to simulate the human cerebrovascular tree. Specifically, we aim to show firstly how the auto-regulation mechanism can be modelled and secondly how smaller arteries, often not visible by non-intrusive MR studies, can be detected by making use of the results obtained from the computer simulation. Results show the time-varying mass flow in each of the efferent vessels and how collateral vessels are even used in naturally 'balanced' configurations. Copyright © 2003 John Wiley & Sons, Ltd.

KEY WORDS: circle of willis; fluid dynamics; computational model; blood flow; brain imaging

INTRODUCTION

The circle of Willis, a ring-like network of vessels, is a complex arterial structure located on the base of the brain. Its role is, as far as possible, to evenly distribute the oxygenated blood proceeding from the heart throughout the whole of the cerebral mass. When looking at the population, there is a considerable range of possible abnormalities in the anatomical structure of the Circle of Willis, the most relevant ones are indicated in Table I.

An MR image of the Circle of Willis is shown in Figure 1. Should a possible combination of one or many of these arteries become severed, occluded or stenosed a reduction of flow could occur with a concomitant reduction in oxygen to the brain mass. In this event ischaemic damage can occur and the person may suffer stroke-like symptoms. Normally functioning non-ideal arterial configurations of the Circle of Willis are not uncommon however with the person living a natural and healthy lifestyle. The main goal of the project is to determine the blood flux and other flow characteristics through the efferent or outlet vessels of the system when

---

* Correspondence to T. David, Department of Mechanical Engineering, University of Canterbury, Private Bag 4800, Christchurch, New Zealand.
† E-mail: tim.david@canterbury.ac.nz, web page: http://www.mech.canterbury.ac.nz/people/td.htm
‡ E-mail: m.d.brown@leeds.ac.uk, Web page: http://leva.leeds.ac.uk/www/staff/index_academic.html
§ E-mail: Alfonso_Ferrandez@scee.net

Table I. Common Abnormalities of the Circle of Willis.

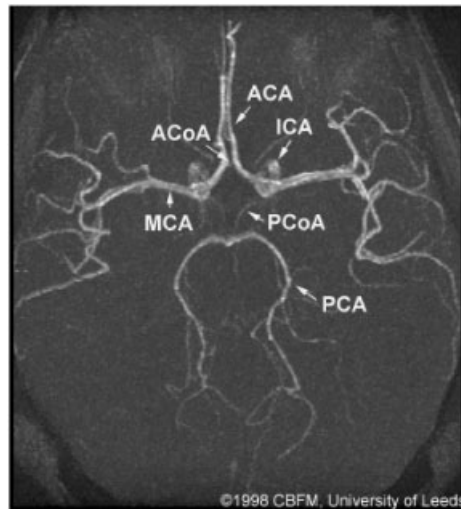| Hypoplastic/Absent	Population
Proximal Anterior Cerebral Artery	25%
Posterior Communicating Artery	22%
Proximal Posterior Cerebral Artery	15%

Figure 1. Magnetic Resonance Image of the Circle of Willis.

the afferent or inlet vessels are set to emulate different pathologies, e.g. mild to severe stenosis in the ICAs and/or variations over time in the arterial blood pressure. At the same time, the behaviour of the model is modified to account for the most common abnormalities. The results of this study showed that the vascular resistance of the brain was of paramount importance when determining the flux distribution.

The cerebro-vascular tree is essentially a series of branching vessels where the daughter vessel diameter is significantly smaller than the parent. In getting smaller the resistance to flow becomes much larger until the arterioles embed themselves at the cellular level and enmesh with the venous system. From a numerical modelling viewpoint it is clearly not sensible to model the flow through continual branching down to the arterioles due to computational expense. However the numerical model must provide the correct physiological downstream boundary conditions since this determines the uniqueness of the solution.

Hillen has developed a number of 1D models of the Circle of Willis [1, 2] as well as using a simple vascular resistance model to produce 1D time-dependent flow profiles [3]. Ferrandez et al. [4] developed a new numerical algorithm for modelling constant vascular resistance in their 2D models of the Circle of Willis. They used porous blocks to represent the downstream peripheral resistance of the vascular tree over middle, anterior and posterior sections of the brain. However these resistances were constant and did not vary as a function of local mass flux. Kufahl and Clark [5] provided a one-dimensional finite difference formulation for flow

in the circle of willis utilizing a constant downstream boundary condition consisting of a combined resistance/capacitance/resistance module.

For normal functioning the brain requires a steady flow of oxygenated blood and nutrients. Given the previous comments concerning vascular resistance the afferent vessels of the cerebro-vascular tree should be at a constant pressure relative to the venous state. However even in normal healthy circumstances the pressure at the internal carotid artery can vary over a relatively large range when the height of the brain varies with respect to the heart, such as lying down or standing up. In order to maintain a constant supply of nutrients to the brain mass the vascular network varies the resistance to flow by dilating or constricting its vessels, this is termed auto-regulation.

The self-regulating mechanism however does not work over all pressure ranges, importantly for hypertensive situations the regulation ceases and any further increase in pressure brings about a proportional increase in the blood flow. A similar phenomenon occurs for hypotension, where decreasing pressure below a certain value induces lower and lower blood flow.

A 2D model has been used since this essentially defines the basic geometry and is the simplest system for CFD flow modelling. 2D geometry was used in this case to ensure that the auto-regulation algorithm (active boundary conditions) could be used with a commercial CFD code. Although the 2D model would give possible non-physiological local flows (recirculation etc.) the efferent fluxes would be physiological. It is excepted that 3D modelling would be 'ideal' however the generation of patient specific geometry from clinical data (e.g. MRI) is a particularly difficult task.

Due to the relatively small vessel diameter and low flow the Reynolds number in cerebro-vascular flow is such that laminar flow can be assumed. Additionally, although there is some compliance in the major components of the cerebro-arterial tree this is relatively small and the major arteries in the brain are considered for the present case to be rigid. The mean shear rate is however relatively high and thus we can assume a Newtonian fluid. By choosing appropriate length, time and velocity scales we may write the non-dimensional time-dependent fluid flow equations for the problem.

The conservation of mass is given as

$$\frac{\partial \rho}{\partial t} + \nabla \cdot \rho \mathbf{u} = 0 \tag{1}$$

whilst the conservation of momentum in Cartesian co-ordinates is

$$\rho \frac{\partial \mathbf{u}}{\partial t} + \rho \mathbf{u} \cdot \nabla \mathbf{u} = -\nabla p + \frac{1}{Re} \nabla^2 \mathbf{u} \tag{2}$$

The previous two equations are the well known Navier–Stokes equations and here

$$Re = \frac{U_\infty R_0}{v}$$

is the Reynolds number, where U_∞, v and R_0 are chosen to be the time-averaged mean velocity in the carotid artery, the kinematic viscosity of blood and the radius of the middle cerebral artery, respectively. In this work we utilized a 2D representation of the full Circle of Willis shown in Figure 2.

In this case we have imposed a 'no-slip' velocity condition on the arterial walls and a prescribed pressure at the inlet (or afferent artery). The outlet or efferent artery, as described
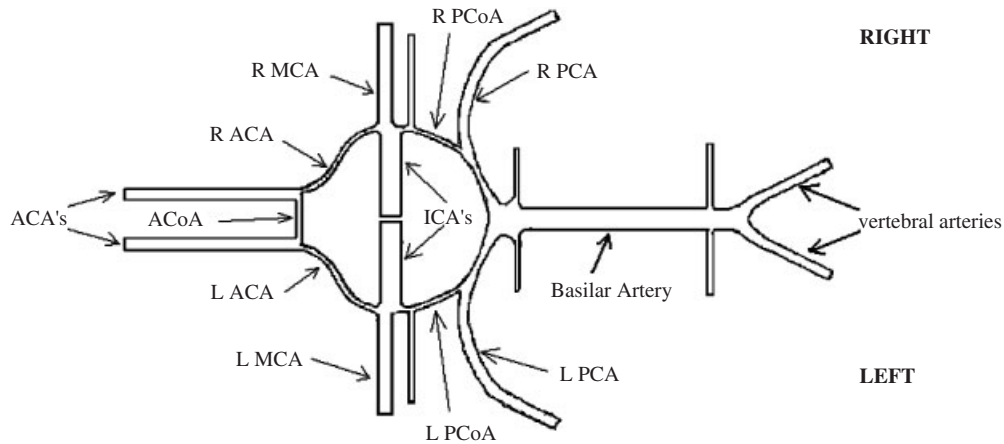
Figure 2. 2D Computational domain of the Circle of Willis.

earlier requires some further detail since we are required to model the peripheral resistance and the auto-regulation.

ACTIVE PERIPHERAL RESISTANCE MODEL

The peripheral vascular bed can be viewed on a macro scale as being a random distribution of interstitial pores. The statistical distribution of arterial diameters across the peripheral system can be associated with the porosity of the porous bed and the ease with which blood flows for a constant pressure difference from the systemic to the venous system can be associated with the porous bed's permeability. Further details can be found in the work by Ferrandez [4] and David, Brown and Ferrandez [6].

In order to dynamically alter the effective resistance of the outlet in the numerical domain we need to define a relationship between the mass flux through the outlet and the permeability. We use a single tube of height h whose inlet flow is of parabolic form with the inlet pressure is given as P_i. Situated at the outlet is a porous block whose length is ε and such that the entire pipe length is $L + \varepsilon$. Since the flow is parabolic and constant in time we can assume that it is driven by a constant pressure gradient. It is easy to show [7, 8] that for a prescribed mass flow rate, q, the permeability k may be evaluated as

$$k = \left[\frac{h\rho}{\varepsilon\mu q}(P_i - P_o) - \frac{12L}{\varepsilon h^2} \right]^{-1} \tag{3}$$

The above result now allows us to impose the required value of permeability k of the porous block so as to obtain the desired mass flow rate q without knowing the pressure P at the interface of the porous block and fluid domain. Hence a position upstream of the porous block is chosen to denote P_i and P_o remains constant since this is the venous return pressure. P_i is determined at each time step from the CFD simulation.

From a simplistic standpoint, auto-regulation is the process that occurs when the amount of flux $q(t)$ through an artery deviates ostensibly from its 'standard' or reference value $q_{ref}(t)$. However small changes in flux are essentially filtered out by the nervous system since this would mean a constant variation in vessel peripheral resistance due to the pulsatility of the blood flow. We define an error in the blood flux to a particular efferent vessel as

$$v(t) = q(t) - q_{ref}(t) \tag{4}$$

and use a standard proportional integral controller which provides a non-zero output $u(t)$ for any changes occurring over preset parameters. This is essentially governed by the integral equation

$$k_i \int v(t)\,dt + k_p v(t) = u(t) \tag{5}$$

where the integral and proportional constants k_i and k_p, respectively, are chosen to approximate physiological conditions, in this case clinical data obtained by Newell *et al.* [9]. This equation can also be thought of as evaluating the correct offset error. In a similar manner we provide a differential equation which models the variation of resistance in response to a non-zero error. The resistance value $y(t)$ is proportional to the input signal. The modification of vascular tone takes a finite time and this must be taken into account along with the characteristic time of the system as a whole. Hence, we may write

$$\tau \frac{d}{dt} y(t) + y(t) = u(t) \tag{6}$$

here τ is the time constant of the simple dynamical system again this value was chosen to simulate the data by Newell *et al.* [9]. Finally the system is limited in the range of vascular peripheral resistance values as is the case in the human, thus $y(t)$ is such that $R_{min} \leqslant y(t) \leqslant R_{max}$. We use a bi-linear z transform to provide a discrete version of Equations (5) and (6). Variations in $y(t)$ are made proportional to variations in the permeability of the porous block as described above. The system as described above is linked to the CFD code via a user-defined function, which evaluates the appropriate porous block permeability condition. A more detailed description of the algorithm can be found in Ferrandez *et al.* [6].

NUMERICAL METHODS AND BOUNDARY CONDITIONS

The above conservation Equations (1) and (2) were solved using the commercial CFD software Fluent for both cases presented below. The dynamic outlet boundary conditions as defined by equations were coded and linked, as a series of user defined subroutines, with the Fluent code at run time. Each individual outlet was treated independently with its own subroutine and all code was written in C. The system was treated as a fully time-dependent simulation and before any pressure variations were simulated the model was allowed to reach equilibrium values starting from an initial state of zero flow through the whole numerical domain.

Ideal circle of Willis (*balanced configuration*)

The fluid domain for the numerical simulation was the same as that used by Ferrandez *et al.* [6] and is shown in Figure 2. Using the specified parameter values of k_i k_p and τ

the dynamic peripheral resistance algorithm and associated CFD model was used to simulate a simple pressure drop (equivalent to 17 mmHg) in the right internal carotid artery (ICA) which simulates a rapid compression of the right ICA. From a clinical stand point, this sudden drop in arterial blood pressure can be achieved in an experimental setting by using a standard 'thigh cuff test' as used by Newell *et al.* [9]. This pressure drop was imposed on a 'steady' flow profile without cardiac pulsatility. It was felt that this was a reasonable profile since the main aim here was to investigate the effect of *mean* pressure drops.

A variety of different geometry variants of the Circle of Willis was investigated in order to obtain an estimate of the worst and best cases. These results can be compared directly with those of Ferrandez *et al.* [6] where the peripheral resistance was held constant. All flux values have been non-dimensionalized by the flux of the internal carotid artery for a 'healthy' and balanced configuration using a mean systemic pressure of 90 mmHg. Peripheral resistance limits as noted above have been set to a range that is based on a percentage of the corresponding reference value R_{ref}. Thus for each artery

$$(1 - 0.95)R_{ref} \leqslant R \leqslant (1 + 0.95)R_{ref} \tag{7}$$

These limits are within observed results found in the literature [9–11].

RESULTS AND DISCUSSION

In testing the auto-regulation algorithm we used the experimental data from Newell *et al.* [9] and found that the dynamic peripheral resistance parameter values of $k_i = -0.02$; $k_p = -0.06$; $\tau = 10$ s gave excellent agreement [4, 6].

Balanced configuration

For the case of a balanced configuration Figure 3(a) shows the normalized flux as functions of time for the ipsilateral efferent arteries (same side as the compressed right side). Whilst those of the contralateral efferent arteries (opposite to the compressed right side) are shown in Figure 3(b).

Several observations can be made from Figures 3(a) and 3(b). The magnitude of the initial loss of flux after the pressure drop seems to be proportional to the pathlength distance from the particular efferent artery to the source of the disturbance, in this case the right ICA. Thus, the right MCA, which is normally found directly opposite the ICA, is subjected to an initial drop in flux of about 18% of its original value. The ipsilateral anterior cerebral artery (ACA) has a 12% initial drop while the ipsilateral posterior cerebral artery (PCA) has only a 9% loss. It can be seen that there is a small overshoot in the flux for the ACA. This occurs because the right ACA demands more flux and so reduces its peripheral resistance whilst also being helped by the left (contralateral) ACA. After approximately 6 s from the onset of the pressure drop all arteries have ipsilateral arteries have returned to their reference values.

For the contralateral side, depicted in Figure 3(b) we see a similar effect with the initial drop somewhat smaller in magnitude to that for the ipsilateral efferent arteries. Here the contralateral MCA has an initial drop of less than 1%. The ACA has an initial drop of approximately 5% and the PCA that of only 3.8%. As before all fluxes return to their reference values after about 6 s.
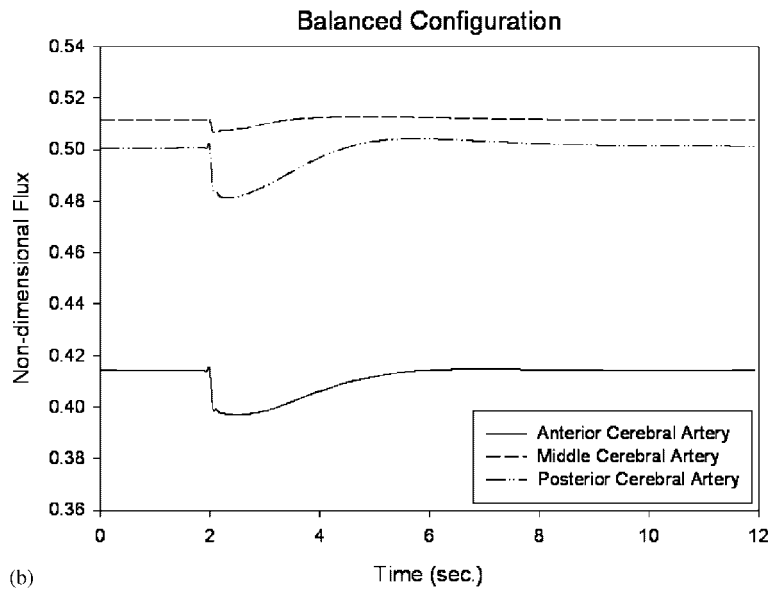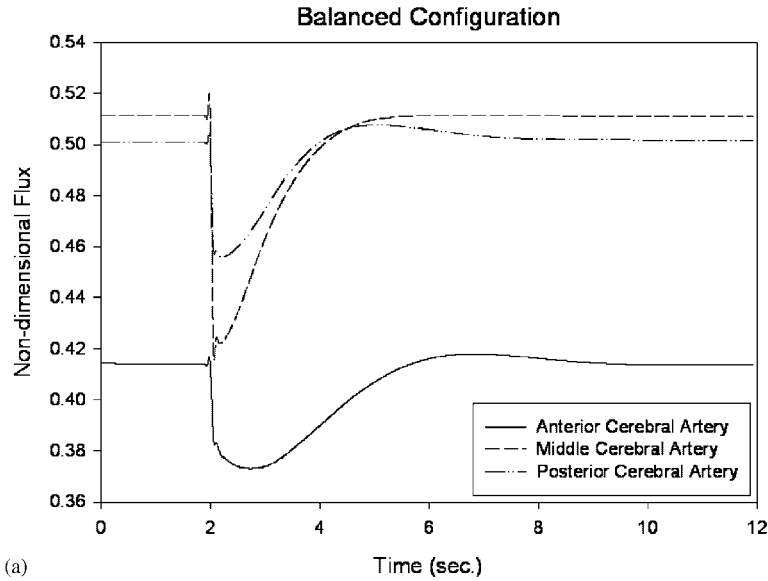
Figure 3. (a) Non-dimensional Flux as a function of time through the ipsilateral ACA, MCA and PCA. (b) Non-dimensional Flux as a function of time through the contralateral ACA, MCA and PCA.

Missing ipsilateral A1 segment of the ACA

From Figure 4(a) the flux response of the ipsilateral MCA and PCA is identical to all previous cases, both in magnitude and time evolution. It is the ipsilateral ACA which seems to have a difficulty in reaching its required reference flux with time. This artery is no longer connected

Missing Ipsilateral A1 Geometry

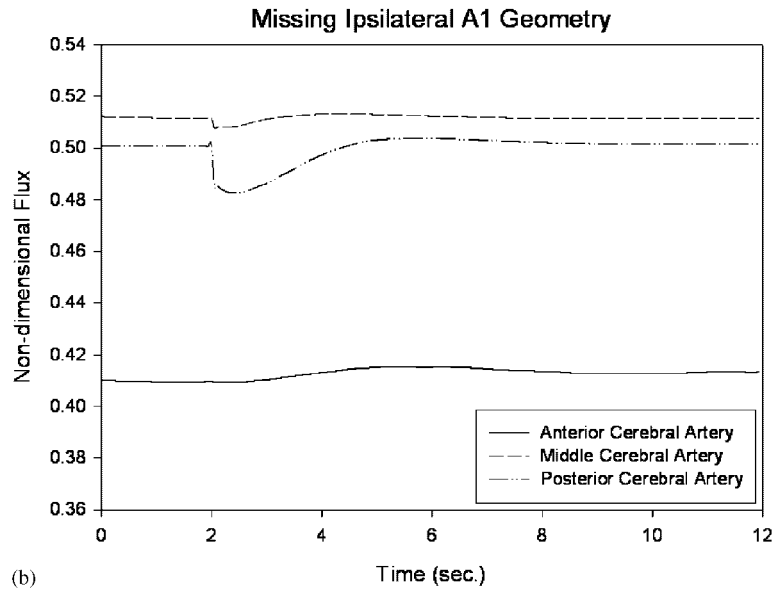(a)

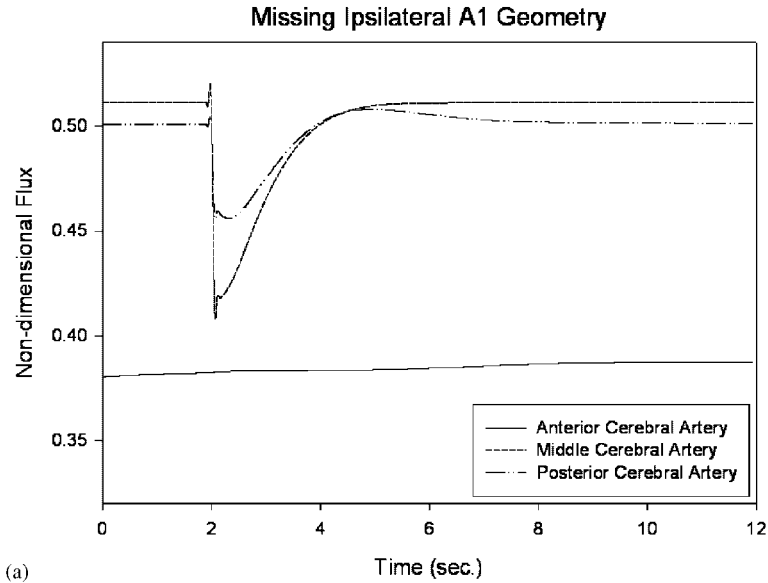## Missing Ipsilateral A1 Geometry

(b)

Figure 4. (a) Non-dimensional Flux as a function of time through the ipsilateral ACA, MCA and PCA.
(b) Non-dimensional Flux as a function of time through the contralateral ACA, MCA and PCA.

to the deficient area, but is only linked to the circle via the ACoA. It is seen that even before the pressure drop takes place, the flux through the ACA is 10% below its non-dimensionalized reference value of approximately 0.418.

Given the limit imposed in the range of resistances that each artery can attain it is clear that the limit set for this particular case has been reached. As a further observation, it appears as if the artery is slightly increasing in flux value before the drop in pressure takes place. This is an artefact resulting from the lower resistance limit being effectively reached and therefore producing an extremely slow recovery towards the absolute minimum.

For the contralateral vessels shown in Figure 4(b) the ACA maintains its reference flux throughout the event. The MCA and PCA have small perturbations to their reference values and are not significantly different from the normal case.

Missing Contralateral A1 segment

The situation where the contralateral A1 segment of the anterior cerebral artery is missing presents an interesting and important result. On the ipsilateral side the fluxes through the MCA and PCA, shown in Figure 5(a) are similar to the previous two cases in that the initial drop is 18% and 9%, respectively.

This anatomical variation presents important challenges to the anterior part of the brain. This is so because both ACAs are solely dependent on the right side of the circle, which is also the one affected by the pressure disturbance.

In fact, we could expect the contralateral ACA to be grossly affected by the change, since after the pressure drop, its only source of flux will be the posterior side of the circle, via the ipsilateral PCoA and then the ACoA, a very long and tortuous route with many other efferent arteries to be supplied before it. Before investigating the contralateral side we see that this case is somewhat different since the overshoot on the ipsilateral ACA is much larger than the previous cases.

Investigation of the contralateral efferent arterial flux, in Figure 5(b), shows that for the ACA it has already reached maximum vaso-dilation even before any pressure drop is executed. The flux condition worsens after the pressure drop since this time the artery is solely connected to the deficient region and hence after the pressure drop the flux decreases considerably. This results eventually in a reduced flux of only 60% of its reference value. In a clinical condition this is probably a critical state. The alterations of the other vessels, the MCA and PCA are only minor with the flux in the MCA remaining within 0.5% of its reference value and the left PCA only presenting with an initial drop of about 4%. Both arteries return to their reference values after approximately 4 s.

The overshoot of flux occurring in the ipsilateral ACA can now be explained. The overshoot can be seen to occur at the same time as the minimum flux is reached in the contralateral ACA, and hence no more flux will be demanded by it. This extra flux is thence redirected to its predecessor, the ipsilateral ACA. Thus a slight excess flux (about 3%) occurs which is dealt with in exactly the same manner as flux reduction but with an increase in resistance rather than a decrease.

Given the agreement of the model with the results of Newell et al. [9] it now seems possible to use the developed numerical model to investigate clinical cases. Experimental results of the MCA velocity using trans-cranial Doppler of patients can be used to evaluate the three dynamic parameters k_i k_p and τ. The numerical model may then be used to simulate possible scenarios which could not otherwise be carried out for ethical or logistic reasons. These numerical experiments could include the possible simulation of surgical manoeuvres, which may prove crucial depending on the specific condition of the patients Circle of Willis.
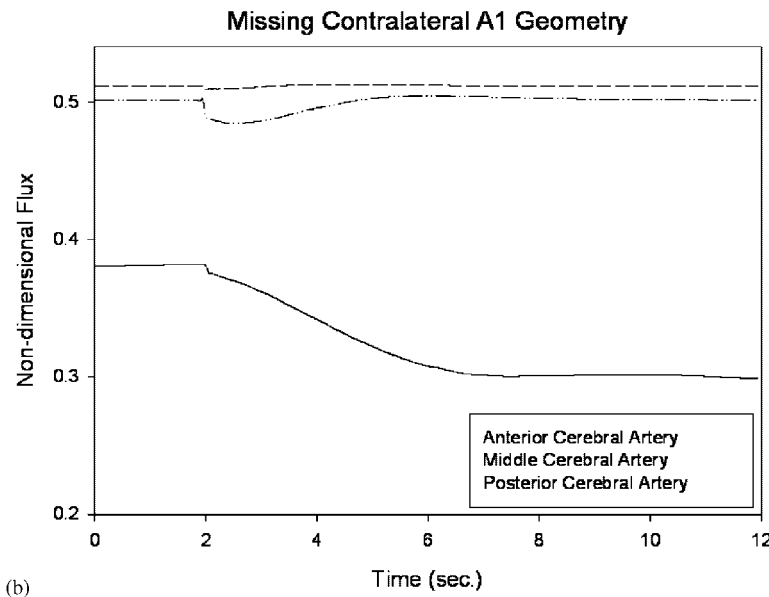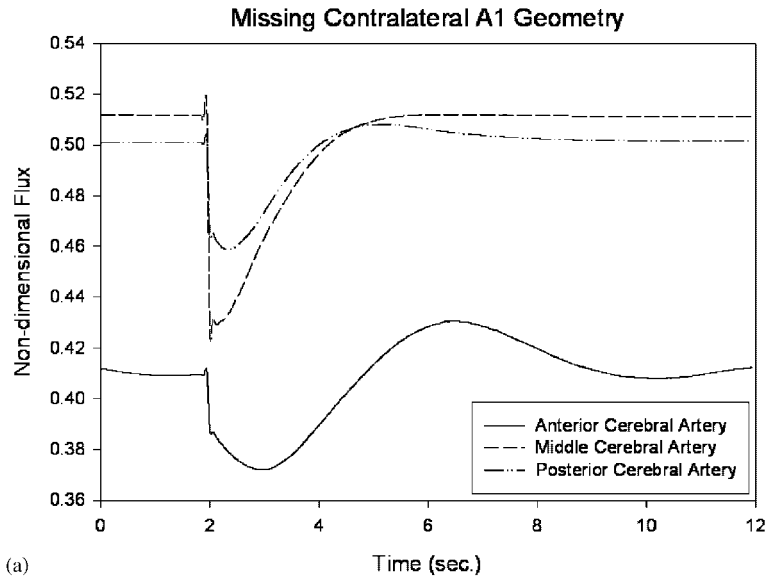
Figure 5. (a) Non-dimensional Flux as a function of time through the ipsilateral ACA, MCA and PCA. (b) Non-dimensional Flux as a function of time through the contralateral ACA, MCA and PCA.

In comparison with a 1D model similar to that of Hillen [2] the additional information from a 2D simulation is not significantly improved. However there are two major advantages to the presented model. Firstly the generation of numerical domains from MR images has become a tool used frequently in numerical modelling of biological fluids and is constantly

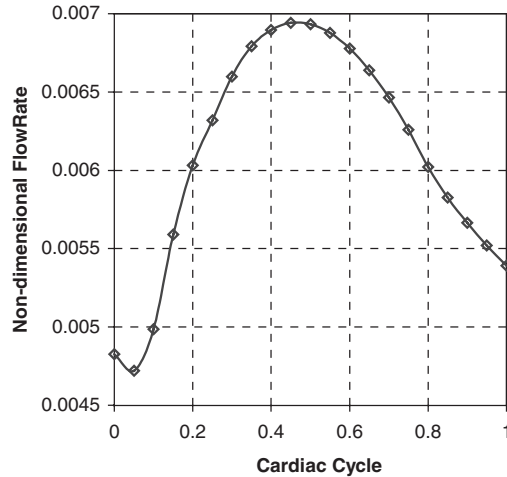　　　　　　　　　　*Int. J. Numer. Meth. Fluids* 2003; **43**:701–713

Figure 6. Posterior Communicating Artery non-dimensional flow rate over the full cardiac cycle.

being developed. This means that patient specific geometry may be readily used. Secondly, the upgrading of the presented CFD model to 3D is relatively easy. No additional work is necessary for the dynamic resistance algorithm.

Finally the parameters k_i k_p and τ and peripheral resistive limits may easily be altered to investigate conditions of both hypo/hyperoxic and hypo/hypertension.

The use of standard MR phase contrast techniques fails to show the Posterior Communicating Arteries (PCoAs) of the Circle of Willis in a considerable percentage of patients, as shown in Figure 1. In some cases, this can lead to misdiagnosis and hence to the modification of the prescribed treatment.

Collateral flow

In addition to auto-regulation studies the present work shows how the numerical simulation can be used to explain why the PCoAs do not always present in routine brain MR scans in certain patients and how it can provide a possible MR protocol which improves the visibility of the PCoA.

From the computational simulations, it was observed that the PCoAs, in the case where all arteries were present, were rarely used. 1D models have utilized the phenomenon that there exists a delay between maximum flux in the internal carotid compared with the vertebral arteries. When this phase delay was introduced via the inlet pressure waves between the internal carotid arteries (ICA) and the vertebral arteries (VA), some flow was observed through the PCoAs. Even when this delay is introduced, there is very little flow, with a peak flux showing for only a brief period of time within the cardiac cycle. Figure 6 shows the non-dimensional flow rate in the PCoA over the cardiac cycle obtained in this simulation. The flow rate values reached are orders of magnitude below the measurements simulated in the major arteries of the model.

From the above results it can be deduced that, in order to improve the visibility of the PCoAs in a MR scan, this should be performed in a specific point in time, where the flux
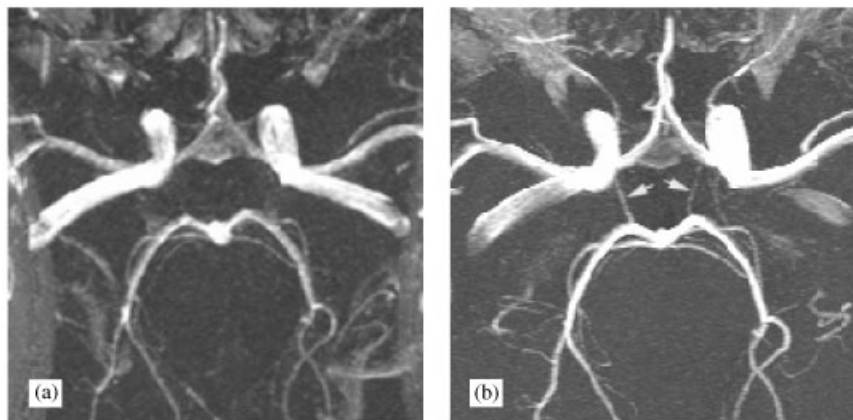
Figure 7. Maximum Intensity Projection of the Circle of Willis using (a) non-gated 3D TOF, and (b) gated 3D TOF. The yellow arrows mark the visible PCoAs.

has been determined to be maximum by the simulation. In this way, the signal obtained by the scanner will appear brighter if and where the PCoAs are present. This would bypass the implicit 'time averaging' that a non-triggered scan employs.

A preliminary study carried out at the MR-Centre of Aarhus University Hospital in Denmark on three healthy volunteers showed an improvement in the ability to detect the PCoAs when a triggered 3D Time of Flight sequence was used, as opposed to the normal non-triggered sequence. However further work using the computational model will be necessary to investigate the relationship between maximum flux in the PCoA and the delay in the pressure wave between vertebral and internal carotid arteries.

Figure 7 shows a Maximum Intensity Projection of the Circle of Willis using (a) Non-Gated 3D TOF, and (b) Gated 3D TOF, the arrows mark the visible PCoAs. In addition the ophthalmic arteries can clearly be seen.

The use of advanced computer simulations of physiological systems, such as the cerebral circulation can shed light into certain processes where their possible causes were hidden or simply not well understood. The particular case discussed here shows that the low visibility of small cerebral arteries when using traditional non-triggered MR techniques can be greatly improved by adapting these scanning techniques to the fluid flow phenomena observed in the computer model. Some authors findings point to a higher completeness of the CoW in patients with carotid disease than in healthy volunteers [12]. The present study has shown that this is not necessarily the case, and that in fact, the carotid obstruction forces blood flow through vessels that otherwise are only used for a small fraction of the cardiac cycle, thus increasing their visibility when using standard non-gated MR imaging techniques.

Therefore, the use of appropriate MR imaging techniques must be assessed before basing diagnostic conclusions in the resulting images. Utilising computational simulations of the circle of Willis has successfully proven that this is in fact the case for the PCoAs. However, further research must be conducted to investigate the relationship between maximum flux in the PCoA and the delay in the pressure wave between the internal carotid and vertebral arteries. This will help determine the optimal time settings for the trigger delay in the acquisition sequence,

therefore enhancing the visibility of these small arteries. In theory, it could then be possible to establish a modus operandi to visualise smaller, more conflictive arteries. This in turn should improve the accuracy of the diagnostic process and reduce the time required to analyse the images.

CONCLUSION

We have developed a dynamic 2D time-dependent simulation of the blood flow in the Circle of Willis. In particular a new type of 'active' outlet boundary condition modelling both peripheral resistance and auto-regulation has been defined and developed. We have shown that the extension to 3D is relatively easy thus enabling patient specific geometry of the Circle of Willis (emanating from MR measurements) to be used and the relevant physiological conditions such as hypertension to be simulated. The model shows the important relationship between geometrical variations and peripheral resistance.

The present work shows how a numerical simulation can be used to explain why the PCoAs have poor visibility in certain patients and how it can also provide guidelines in devising a different MR protocol to improve the results of the imaging process.

REFERENCES

1. Hillen B, Gaasbeek T, Hoogstraten HW. A Mathematical Model of the Flow in the Posterior Communicating Arteries. *Journal of Biomechanics* 1982; **15**(6):441–448.
2. Hillen B, Hoogstraten HW, Post L. A Mathematical Model of the Flow in the Circle of Willis. *Journal of Biomechanics* 1986;**19**(3):187–194.
3. Hillen B, *et al*. Analysis of Flow and Vascular Resistance in a Model of the Circle of Willis. *Journal of Biomechanics* 1988; **21**(10):807–814.
4. Ferrandez A. Computational Models of Blood Flow in the Circle of Willis. In *School of Mechanical Engineering*. University of Leeds: LEEDS, U.K., 2001.
5. Kufahl RH, Clark ME. A Circle of Willis Simulation Using Distensible Vessels and Pulsatile Flow. *Journal of Biomechanical Engineering* 1985; **107**:112–122.
6. Ferrandez A, David T, Brown M. Numerical Models of Auto-regulation and Blood Flow in the Cerebral Circulation. *Computer Methods in Biomechanics and Biomedical Engineering* 2002; **5**(1):7–20.
7. Batchelor GK. *An Introduction to Fluid Dynamics*. Cambridge University Press: Cambridge, UK, 1967.
8. Ferrandez A, *et al*. Computational Models of Blood Flow in the Circle of Willis. *Computer Methods in Biomechanics and Biomedical Engineering* 2000; **4**:1–26.
9. Newell DW, *et al*. Comparison of Flow and Velocity during Dynamic Autoregulation Testing in Humans. *Stroke* 1994; **25**:793–797.
10. Gao E, *et al*. Mathematical Considerations for Modelling Cerebral Blood Flow Autoregulation to Systemic Arterial Pressure. *American Journal of Physiology* 1998; **274**:1023–1031.
11. Mancia G, Mark AL. *Arterial Baroreflexes in Humans. Handbook of Physiology*, Section 2. American Physiological Society, 1983.
12. Hartkamp MJ, *et al*. Circle of Willis Collateral Flow Investigated by Magnetic Resonance Angiography. *Stroke* 1999; **30**(12):2671–2678.

Int. J. Numer. Meth. Fluids 2003; **43**:701–713